Simultaneous Determination of Thermal Conductivity and Heat Capacity in Thin Films with Picosecond Transient Thermoreflectance and Picosecond Laser Flash

Zefang Ye^a, Janghan Park^a, Xianghai Meng^a, Jung-Fu Lin^{b,c*} and Yaguo Wang^{a,c*}.

^a Department of Mechanical Engineering, The University of Texas at Austin, Austin, TX, USA; b Jackson School of Geosciences, The University of Texas at Austin, Austin, TX, USA; c Texas Materials Institute, The University of Texas at Austin, Austin, TX, USA

CONTACT: Yaguo Wang yaguo.wang@austin.utexas.edu; Jung-Fu Lin afu@jsg.utexas.edu

Simultaneous Determination of Thermal Conductivity and Heat Capacity in Thin Films with Picosecond Transient Thermoreflectance and Picosecond Laser Flash

Abstract: Combining the picosecond transient thermoreflectance (ps-TTR) and picosecond laser flash (ps-LF) techniques, we have developed a novel method to simultaneously measure the thermal effusivity and the thermal diffusivity of metal thin films, and determine the thermal conductivity and the heat capacity altogether. In order to validate our approach and evaluate the uncertainties, we analyzed five different metal films (Au, Cu, Ni, Pt, and Ti) with thicknesses ranging from 297nm to 1.2μm. Our results on thermal transport properties and heat capacity are consistent with literature values, with the uncertainties for the thermal conductivity and the heat capacity measurements about $\pm 16\%$ and $\pm 8\%$, respectively. Comparing with the ps-TTR technique alone, the combined approach substantially lowers the uncertainty of the thermal conductivity measurement. Uncertainty analyses on various materials show that that this combined approach is capable to measure most of the materials with a wide range of the thicknesses, even down to 43nm for low thermal conductivity materials (e.g. mica). Simultaneous measurement of thermal conductivity and heat capacity enables exploration of thermal physical behaviour of materials under various thermodynamic and mechanical perturbations, with potential applications in thermal management materials, solid state phase transitions, planetary sciences, and beyond.

Keywords: picosecond transient thermoreflectance, picosecond laser flash, thermal conductivity, heat capacity

In-situ thermal properties characterization is critical for a broad range of scientific fields, including but not limited to thermal management, phase transition in solid state physics, as well as Earth and planetary science, etc. Accurate determination of both c_v and k during a phase transition is crucial for estimating the thermoelectric figure-of-merit and ensuring proper thermal management. In general, high thermal conductivity materials are more efficient at transferring heat away from heat generation area, thus help avoid overheating and improve overall performance and reliability, while high heat capacity helps stabilize the device's temperature. Thus, adding a layer of material with both high heat conductibility and high heat storage ability

would further benefit the thermal management. In solid state physics, c_v , the second-order derivative of the thermodynamic Gibbs free energy, provides information about the nature of phase transition, including the type of phase transition and the critical temperature. For instance, c_v displays singularity at the critical point for the first-order phase transition which reflects the latent heat -- the absorption of energy without any temperature change [1]-[3]. While in certain types of second-order phase transition such as paramagnetic to ferromagnetic transition and superconducting transition, c_v experiences an anomaly near the critical point [4]–[7]. Simultaneous determination of c_v and k can reveal the charge carrier and lattice vibration behaviours near the phase transition. In the fields of Earth and planetary sciences, c_v and k are crucial parameters to calculate the temperature and heat flux distribution in the interior of the Earth and other planets. In the lower mantle the Earth, the adiabatic temperature profile can be determined by $(\frac{dT}{dz})_s = \frac{\rho_m g \alpha_{th} T}{\rho_c c_P}$, where the isobaric heat capacity (c_P) plays the essential role and can be converted from isochoric heat capacity (c_v) [8], [9]. Additionally, thermal conductivity at high pressure is important in predicting the heat transport within the Earth interior. Recent research on high κ of stishovite under extreme pressure has revealed that the subducted basaltic materials are more thermally conductive than previously thought, resulting in the geodynamic anomalies around that area [10]. In the realm of thermodynamics, the measurement of heat capacity can be converted to the Grüneisen parameter (γ) which is defined as $\gamma = \alpha K_T / \rho c_v$ [11]. The Grüneisen parameter is an importance factor in Mie-Grüneisen equation of state (EoS) [12], [13], which provides a framework for predicting the thermodynamic properties of materials, especially metals, under shock wave conditions [14], [15]. Moreover, combined with the Lindemann's criterion [16], γ is crucial to the calculation on the P-T melting curves of the materials such as iron, which is still a controversial topic [17]. Precise measurement of the heat capacity and thermal conductivity, and subsequent determination of the Grüneisen parameter can provide important insights into thermodynamic behaviours of materials under extreme conditions.

Even though thermal conductivity and heat capacity are the two of the most common and important thermal properties for materials, in reality, most optical thermoreflectance based measurements measure thermal diffusivity ($\alpha = \kappa/c_v$) or effusivity ($\varepsilon = \sqrt{c_v \kappa}$) and convert them to thermal conductivity (or heat capacity) with literature heat capacity (or thermal

conductivity) [18], [19]. The thermal diffusivity is related to the heat propagation rate inside the material, while thermal effusivity reflects how heat is exchanged between the sample and its surrounding materials. Whether α or ϵ is measured depends on specific techniques. A traditional laser flash method uses a strong continuous wave (CW) light source to shine on one side of the sample, and an IR thermometer or a thermal couple to monitor the temperature increase on the other side [19], [20], which mainly reflects how fast the heat can propagate inside the sample, hence the diffusivity is obtained. For the bulk material, the thermal diffusivity is easily calculated with the time to the temperature half maximum $t_{1/2}$ and the sample thickness d through $\alpha = 0.1388 \frac{d^2}{t_{1/2}}$ [19]. For thin films, Taketoshi et al. developed the ultrafast laser flash measurement using the picosecond and nanosecond laser as the heating source and the temperature increase on the other side is analytically solved [21]–[24]. From the temperature arising profile, thermal diffusivity can be extracted either using analytical or numerical methods [19], [25]–[27]. With transient thermoreflectance (TTR) [28]–[30], where usually both heating pulse (pump) and detecting light (probe, CW) are on the same side and the probe sits at the center of pump spot, thermal effusivity is measured because the probed signal reveals how fast the heat escapes from the heated location to the surrounding. For time-domain thermoreflectance (TDTR) [18], [31] and frequency-domain thermoreflectance (FDTR) [32], [33], what is measured depends on the heat penetration depth (d_{th}) with respect to thickness of the target layer (d), and d_{th} is controlled by modulation frequency. When d_{th} is much smaller than d and the sample layer can be treated as semiinfinite, the collected signal is sensitive to effusivity. When d_{th} is much larger than d, the whole layer can be treated as interface resistance and the signal is sensitive to diffusivity.

Note that heat capacity can be determined separately with differential scanning calorimetry/thermogravimetric analysis (DSC/TGA) method [34], [35], but the powder form of samples is usually required. Although there are devices developed for measuring heat capacity in thin films, their fabrication can be quite complex, making them unsuitable for use with many materials. For low-dimensional materials, usually the heat capacity of bulk counterparts is used, and its validity is still questionable. In extreme environments, such as high temperature or high-pressure cases, both the heat capacities and the thermal conductivities of most materials are not available. Although some frequency-dependent TDTR and FDTR can also measure the thermal

conductivity and heat capacity together [32], [36], the FDTR is not a suitable technique when thermal diffusivity is lower than $3 \times 10^{-6} \text{m}^2 \text{s}^{-1}$ [32]. With TDTR, the signal is less sensitive to thermal conductivity when the thickness is smaller than the shortest thermal penetration depth, which is constrained by the maximum modulation frequency [37].

In this work, we combine the ps-TTR [30] and ps-LF [21], [22] techniques to measure thermal effusivity and diffusivity simultaneously and conduct global fitting to obtain both thermal conductivity and heat capacity. Five metal films with thicknesses ranging from 297nm to 1.2 μ m are measured, with κ and c_v values consistent with literature data and uncertainties below $\pm 16\%$ and $\pm 8\%$, respectively. This combined approach offers unique advantages on characterizing thermal properties, especially under extreme conditions, such as in a high-pressure diamond anvil cell (DAC).

The thermal effusivity is obtained with ps-TTR (Fig. 1a) where the pump laser has 15ps pulse duration (full width at half maximum) (Coherent Talisker Ultra 532-8, 1064 nm, 200kHz repetition rate, 1mW) and probe is a CW laser (Coherent Verdi V6, 532nm, CW, 1mW). The pump and probe lasers are positioned on the same side of the sample, with the probe laser spot located at the center of the pump laser spot at the sample surface. A gold transducer layer coated at the probe side of the sample is used to increase the dR/dT ratio ($\sim 2 \times 10^{-4} {\rm K}^{-1}$) and to ensure low absorbance (<0.3) at the probe wavelength (532nm) [38]. The reflected probe is collected with a silicon avalanche photodiode (Hamamatsu C5658) with a time resolution of 500ps and then recorded with an oscilloscope (Tektronics TDS 744A). Since the separation time between pump pulses is 5 micro-second, it is possible to record a comprehensive thermal profile, spanning from the initial temperature to the peak and then to relaxation, without any thermal accumulation effect. The same ps-TTR setup is modified to perform ps-LF measurement (Fig. 1b). The probe laser path remains the same as that of ps-TTR, while the pump laser is routed to heat the sample from the other side. A flip mirror is used to switch the pump beam path for the two measurement geometries. To differentiate the experimental setups, we would continue to name the front-pump front-probe configuration as ps-TTR and the back-pump front probe as ps-LF.

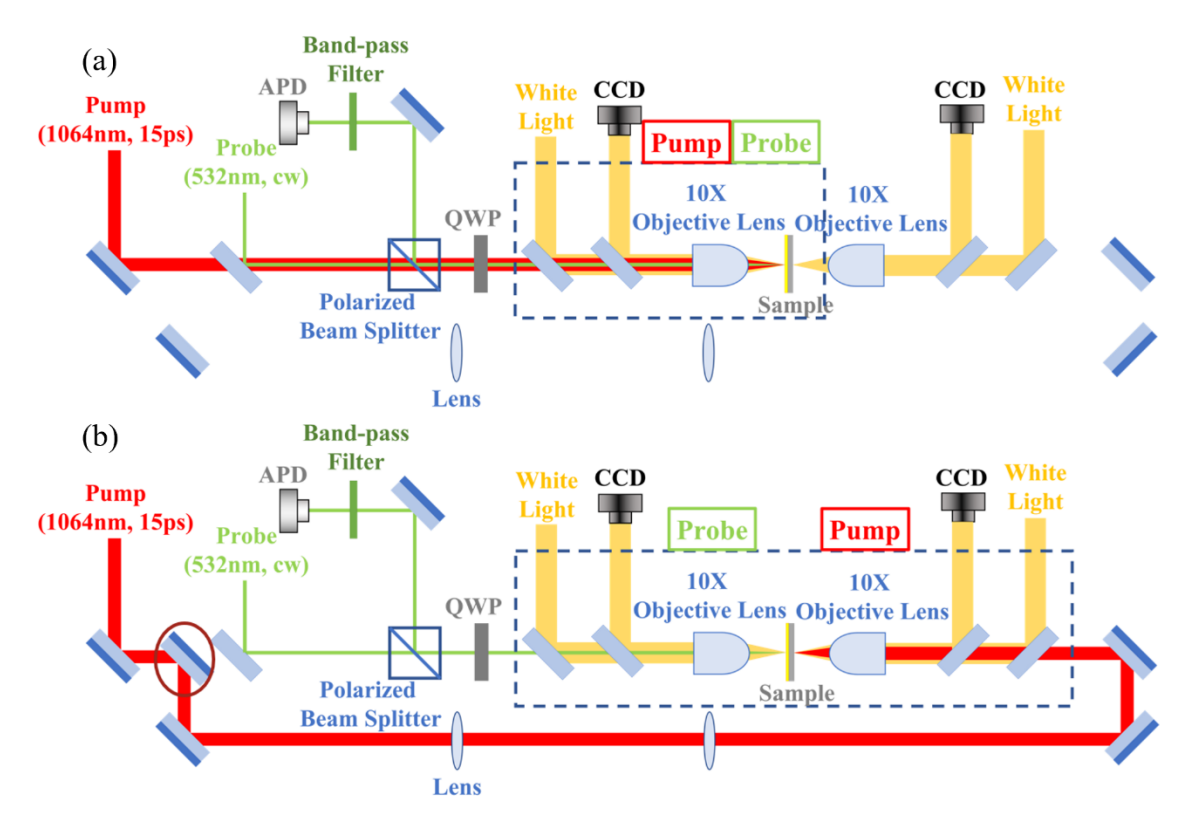


Figure 1. Optical layouts of the (a) ps-TTR and (b) ps-LF systems. The flip mirror (dark red circle) is used to switch the optical path of the pump laser (1064 nm, red lines) between the two systems.

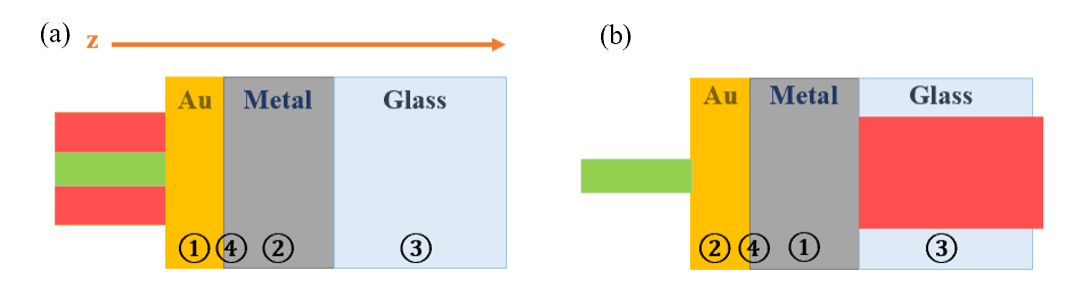


Figure 2. Schematics for the sample configuration and the pump-and-probe geometry for the (a) ps-TTR system and (b) ps-LF system. For the ps-TTR measurement, ① indicates the layer that absorbs the energy of the pump laser and also reflects the CW probe laser. Its temperature profile is described in Eq. 1 with the source term described in Eq. 2. For the ps-LF measurement, the pump energy is absorbed in the metal film near the metal/glass interface. Layer ②③ are the layers that do not absorb the pump, described with Eq. 3. ④ is the interface expressed in Eq. 4.

In both experiments, a 1-D heat conduction along cross-plane direction is assumed, because the pump spot size $(120\mu m, 1/e^2)$ is much larger than the probe spot size $(10\mu m, 1/e^2)$ and the sample layer thickness (up to 1.2 μ m). All samples have the Au/Metal/Glass layered structure (Fig. 2). A multi-layer 1D thermal diffusion model is solved with the finite difference method to simulate both configurations, as described with Eqs. 1 to 4 [29], [39], [40].

$$\rho_{\widehat{1}} c_{\widehat{1}} \left(\frac{\partial T_{\widehat{1}}}{\partial t} \right) = \frac{\partial}{\partial z} \left(\kappa_{\widehat{1}} \frac{\partial T_{\widehat{1}}}{\partial z} \right) + S(z, t)$$
 (1)

$$S(z,t) = \frac{0.94(1 - R_{pump})F}{t_p \delta[1 - \exp(-\frac{L}{\delta})]} \exp\left[-2.77 \frac{(t - 2t_p)^2}{t_p^2} - \frac{z}{\delta}\right]$$
(2)

$$\rho_{i}c_{i}\left(\frac{\partial T_{i}}{\partial t}\right) = \frac{\partial}{\partial z}\left(\kappa_{s}\frac{\partial T_{i}}{\partial z}\right), i = 2 \text{ or } 3$$
(3)

$$-\kappa_{\widehat{1}} \frac{\partial T_{\widehat{1}}}{\partial z} \Big|_{z=interface} = -\kappa_{\widehat{2}} \frac{\partial T_{\widehat{2}}}{\partial z} \Big|_{z=interface} = G(T_{\widehat{1}} - T_{\widehat{2}}) \Big|_{z=interface}$$
(4)

Where ρ is the density, c is the specific heat in Jkg⁻¹K⁻¹, κ is the thermal conductivity, T is the temperature and S is the source term due to pump laser heating. Note that the final volumetric heat capacity extracted from the model is $c_v = \rho c$ Jm⁻³K⁻¹. R_{pump} is the reflectivity of the absorption layer at the pump laser wavelength, F is the laser fluence, t_p is the pulse width, δ is the optical absorption depth, and L is the thickness of the absorbing layer. G is the interfacial thermal conductance between layers.

Five metal samples are measured with this combined approach. Four thin metal films (297nm Nickel, 325nm Chromium, 500nm Aluminum, and 1107nm Titanium) are deposited onto a 160μm-thick glass substrate using e-beam evaporation (Kurt J. Lesker, PVD75) or thermal evaporation (Kurt J. Lesker, NANO36). A 1.2μm Platinum foil is compressed from the Platinum powders (Goodfellow, 99.95% purity) in a high-pressure diamond anvil cell and then placed on the glass substrate. The films and foil thicknesses are determined with a profilometer (Dektak 6M Stylus). All the samples are coated with a 60nm gold layer on the surface as the thermal transducer using thermal evaporation. With ps-TTR, the gold transducer absorbs all pump laser

energy, since the optical penetration depth of gold at 1064nm is 12.2nm, much smaller than the gold layer thickness, so the source term S is only nonzero in the gold layer. The calculated time-dependent temperature profile on Au surface is used to fit the ps-TTR data. With ps-LF, the pump passes through the glass substrate and is absorbed by the metal directly near the metal/glass interface. The optical penetration depths of 1064nm laser in the measured metals are less than 23.7nm, much less than metal layer thickness ranging from 297nm to 1.2 μ m. The calculated temperature rising profile at the Au surface is used to fit the ps-LF data.

With two data sets and two simulated time-dependent temperature curves, we conducted a global fitting with shared parameters using the least squares method. Due to the Au/Metal/Glass structure of our samples, the unknown parameters are the heat capacity (c_n) and the thermal conductivity (κ) of the metal film, together with the interfacial thermal conductance (G) between the gold and the metal film. The input parameters include the heat capacity, the thermal conductivity, and the thickness of the gold and glass layers, and the thickness of the metal films [41], [42]. Plotted in Fig. 3a-b are the normalized fitting curves compared with the normalized experimental data measured in Titanium thin film. With ps-TTR, the criteria for choosing the fitting time range are described in our previous paper, that the time range should maximize the area underneath the sensitivity curve (Fig. 4) [30]. Meanwhile, the fitting time should not be too long where the reflectivity change signal is small, because the low signal-to-noise ratio would induce extra uncertainty on the final fitting result. For all the ps-TTR experiments, we choose the first 100ns as the fitting time range. With ps-LF, the fitting is most sensitive to the temperature rising part, so we choose the signal range where the temperature starts to rise until the temperature reaches its maximum. Along with the experimental data and the best fitting curves, we plot the confidence intervals by varying the fitted c_v and κ values by $\pm 20\%$. For ps-TTR (Fig. 3a, inset), the $\pm 20\%$ κ and $+20\% c_v$ almost overlap with each other, which is consistent with the fact that ps-TTR results are sensitive to the effusivity, the multiplication of κ and c_v . For ps-LF (Fig. 3b, inset), the +20% c_v show a similar trend with -20% κ , indicating that ps-LF results are sensitive to the diffusivity. The fitted κ and c_{ν} values for all five samples are plotted in Fig. 3c-d, against reference values. All the measured values with our ps-TTR + ps-LF approach agree well with literature data, suggesting that this approach is reliable for simultaneous determination of κ and c_v .

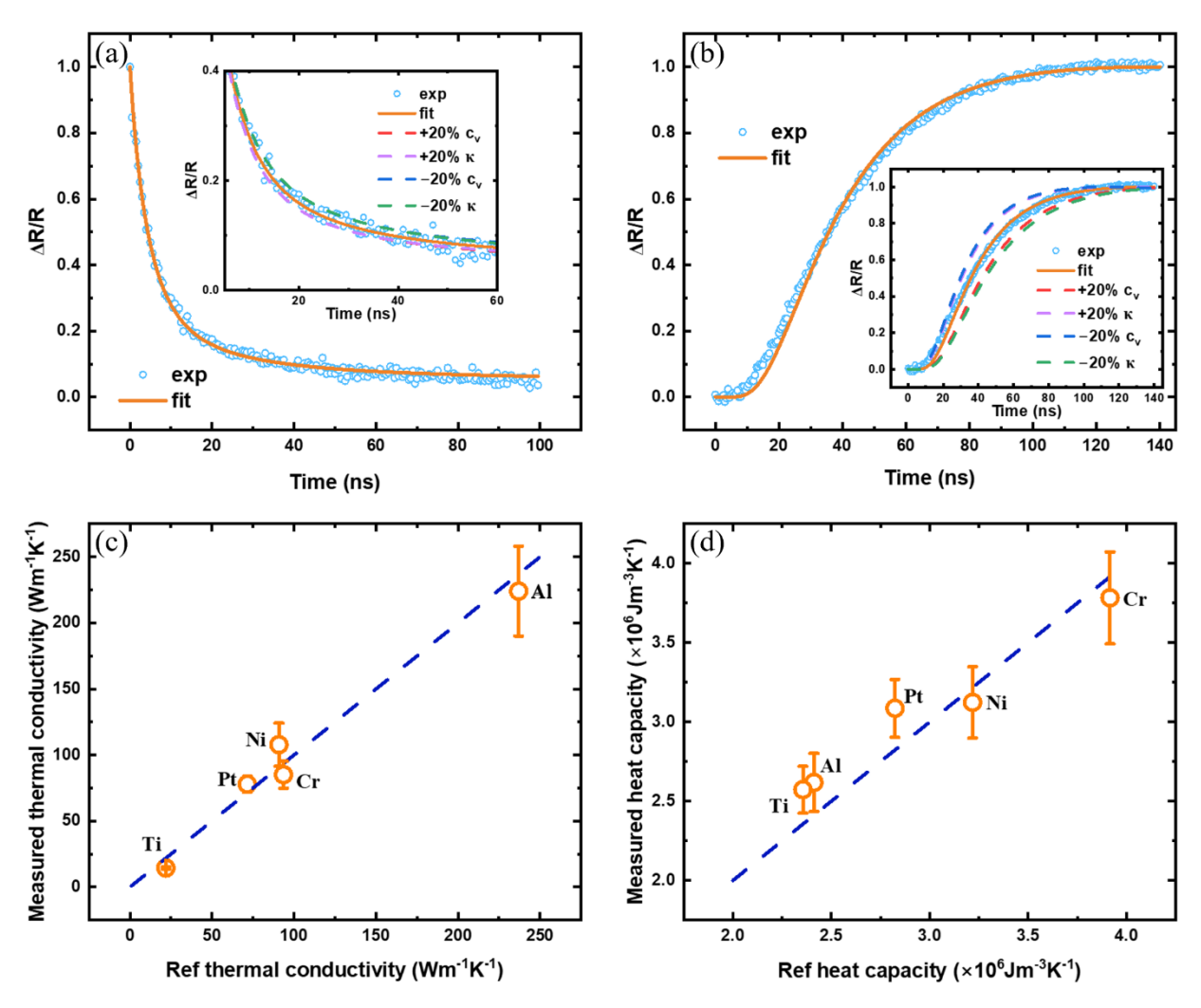


Figure 3. Normalized experimental reflectivity change of probe and simulation curves with best-fitted κ and c_v from (a) ps-TTR and (b) ps-LF measurements. The insets are the simulation curves with 20% variation of the κ or c_v . The best-fitted thermal conductivity (c) and heat capacity (d) are compared with the literature results [41], [43].

Now we want to discuss the sensitivity and uncertainty of this combined approach and compare them with the case of single set data measurement (ps-TTR), as well as other popular techniques. The sensitivity (S) of the model is calculated by evaluating the change in the temperature curve (T) with respect to the change of independent parameters (x_0) : $S = \frac{\partial \ln T}{\partial \ln x_0}$ [44]. According to the Au/Metal/Glass structure of our samples as shown in Fig. 2, the multi-layer model contains three layers and the independent variables are the thickness (d), thermal conductivity (κ) , volumetric heat capacity (c_v) of all three layers, as well as the interface conductance between them (G).

Fig.4a&b show an example of a sensitivity test on Titanium film with 1.1 μ m thickness. In Fig.4a, the sensitivities of the volumetric heat capacity and the thermal conductivity of the Titanium film are both negative in the ps-TTR configuration and follow the same trend until the sensitivity of the thermal conductivity ($\kappa_{z,Ti}$) starts to decrease, at which point the heat passes through the metal layer and reaches the glass substrate. This tendency indicates that when heat travels within the Titanium layer, the thermal response is governed by effusivity ϵ . Higher heat capacity and larger thermal conductivity of the Titanium film would increase the rate of heat dissipation in the gold layer and bring down the surface temperature quicker, therefore the sensitivities are negative. For the case of ps-LF (Fig.4b), the sensitivities of heat capacity and thermal conductivity have opposite trends, because the higher κ leads to faster temperature rising on the back side, while larger heat capacity causes more heat storage in the Titanium layer and slows down the heat propagation. So thermal response for the ps-LF case is governed by the thermal diffusivity α .

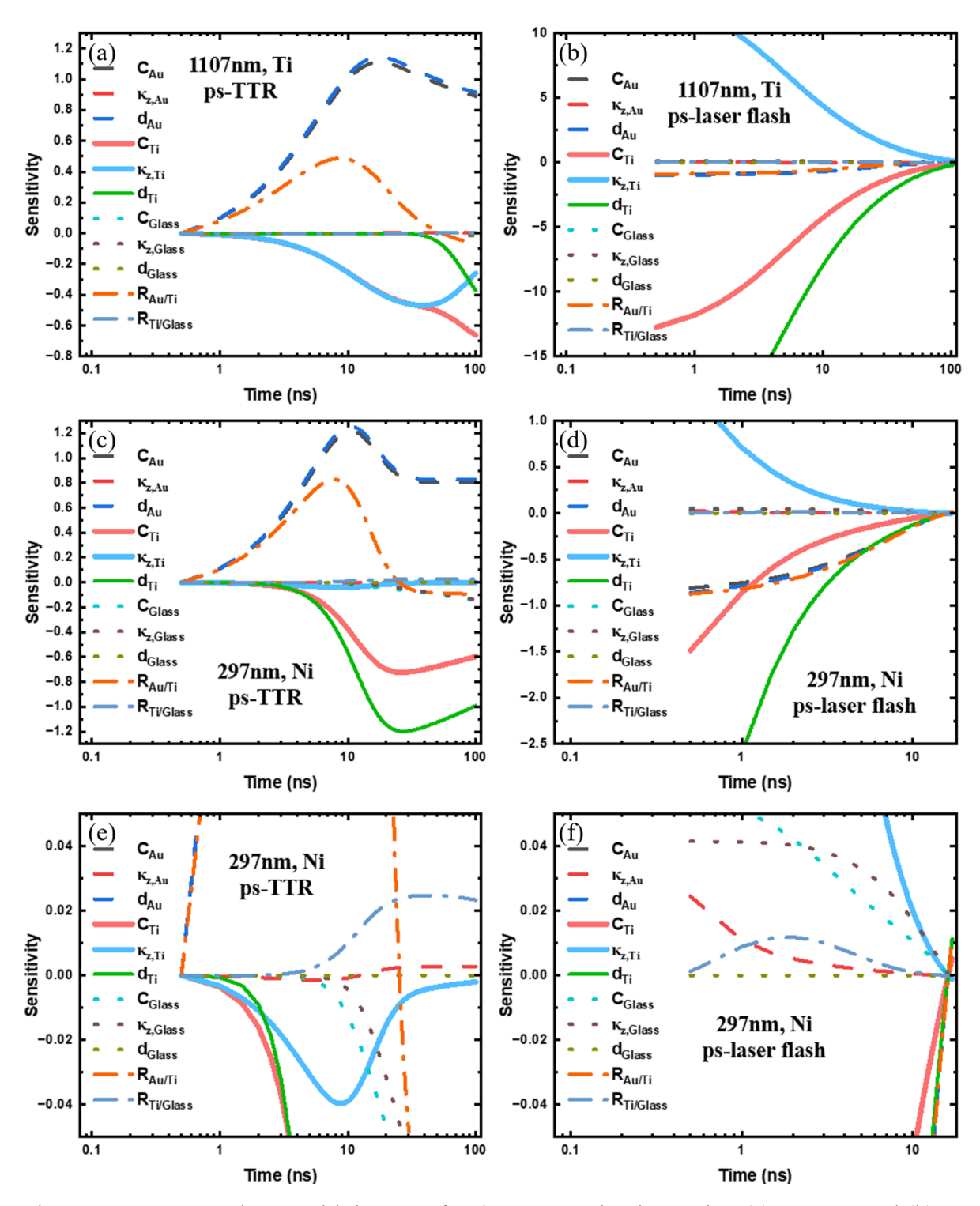


Figure 4. Representative sensitivity tests for the 1.1µm Titanium using (a) ps-TTR and (b) ps-LF, and for 297nm Nickel using (c) ps-TTR and (d) ps-LF. The areas around the zero sensitivity in (c) and (d) are enlarged into (e) and (f), respectively, for clarity.

Fig. 4c-f show the sensitivity of the 297 nm-thick Ni film on glass substrate, the thinnest sample tested. The κ_{Ni} is unlikely to be determined with ps-TTR alone due to that the sensitivity is less than 0.1, however, considered that the large sensitivity of κ_{Ni} and $c_{v,Ni}$ in ps-LF, the κ_{Ni} can be extracted with low uncertainty. One thing worth pointing out is that the sensitivities for the interface resistance between Ti/Glass and the Ni/Glass (Fig. 4) are negligible for both configurations, thus we didn't set this interfacial conductance as a free parameter. Instead, we set the interfacial conductance as a constant: $G_{\text{metal/glass}} = 50 \text{MWm}^{-2} \text{K}^{-1}$, which is around the average value of the metal/glass interfacial resistance we measured previously in the ps-TTR experiments [30], and also similar with the $G_{\text{Au/metal}}$ interfacial conductance we measured in the current experiment.

Fig. 3 c&d plot the measured κ and c_v values along with uncertainties, which are all below $\pm 16\%$ and $\pm 8\%$, respectively, and mainly come from the error propagation of the input parameters and the error of the experimentally measured signal. The overall uncertainties are calculated with the error propagation formula [30], [45]:

$$var[U] = (J_{U}^{T}J_{U})^{-1}J_{U}^{T}var[R_{exp}]J_{U}(J_{U}^{T}J_{U})^{-1} + (J_{U}^{T}J_{U})^{-1}(J_{U}^{T}J_{p})var[P](J_{U}^{T}J_{p})^{T}(J_{U}^{T}J_{U})^{-1}$$
(5)

where U represents the fitting parameters: thermal conductivity, heat capacity and interface conductance. The diagonal elements of the var[U] are the variance of those parameters σ_U^2 . The uncertainty is defined as σ_U , and the actual range of measured value U is U $\pm \sigma_U$. P includes the rest of the input parameters: thermal properties of Au and glass, and thicknesses of all layers. J_U and J_P are the Jacobi matrix, defined as:

$$J_{U} = \begin{pmatrix} \frac{\partial Temp(t_{1})}{\partial u_{1}} & \cdots & \frac{\partial Temp(t_{1})}{\partial u_{l}} \\ \vdots & \ddots & \vdots \\ \frac{\partial Temp(t_{N})}{\partial u_{1}} & \cdots & \frac{\partial Temp(t_{N})}{\partial u_{l}} \end{pmatrix}$$
(6)

$$J_{P} = \begin{pmatrix} \frac{\partial Temp(t_{1})}{\partial p_{1}} & \cdots & \frac{\partial Temp(t_{1})}{\partial p_{1}} \\ \vdots & \ddots & \vdots \\ \frac{\partial Temp(t_{N})}{\partial p_{1}} & \cdots & \frac{\partial Temp(t_{N})}{\partial p_{1}} \end{pmatrix}$$
(7)

Temp here refers to the normalized temperature curve, and $t_1 \cdots t_N$ are the discrete fitting time. In ps-TTR, we usually calculate time-dependent J_U and J_P by varying the t_N and then plot the time-dependent uncertainty [30]. Since we have already fixed the fitting time range in this experiment, we no longer treat J_U and J_P as time dependent. Also, there are two sets of the temperature curves since we have both ps-TTR and ps-LF configurations, they can be simply combined into one temperature vector Temp. The variance matrix of P is diagonal, with elements as the uncertainties of the input parameters, which are set as $\pm 1.5\%$. The uncertainty of Au thickness is set as $\pm 5\%$, which mainly comes from the profilometer measurement error. R_{exp} is the experimental signal, and its variance is set as $\pm 1.5\%$ also.

To compare the uncertainties of this combined approach with the ps-TTR, the uncertainty of the thermal conductivity of the Titanium film is calculated for both ps-TTR alone and the combined method. When only use the experimental data of ps-TTR, the uncertainty of the thermal conductivity is about $\pm 19.83\%$ [30]. While with this combined approach, the uncertainties of thermal conductivity and heat capacity are about $\pm 5.75\%$ and $\pm 5.87\%$, separately. A significantly lower uncertainty is achieved with this combined approach. The main reason for this uncertainty reduction is that the sensitivities of the heat capacity have different signs for ps-TTR and ps-LF, which is originated from the different locations of c_v in the expression of thermal diffusivity and effusivity. When conducting the matrix calculation, terms with different signs would cancel each other, thus leading to lower uncertainty.

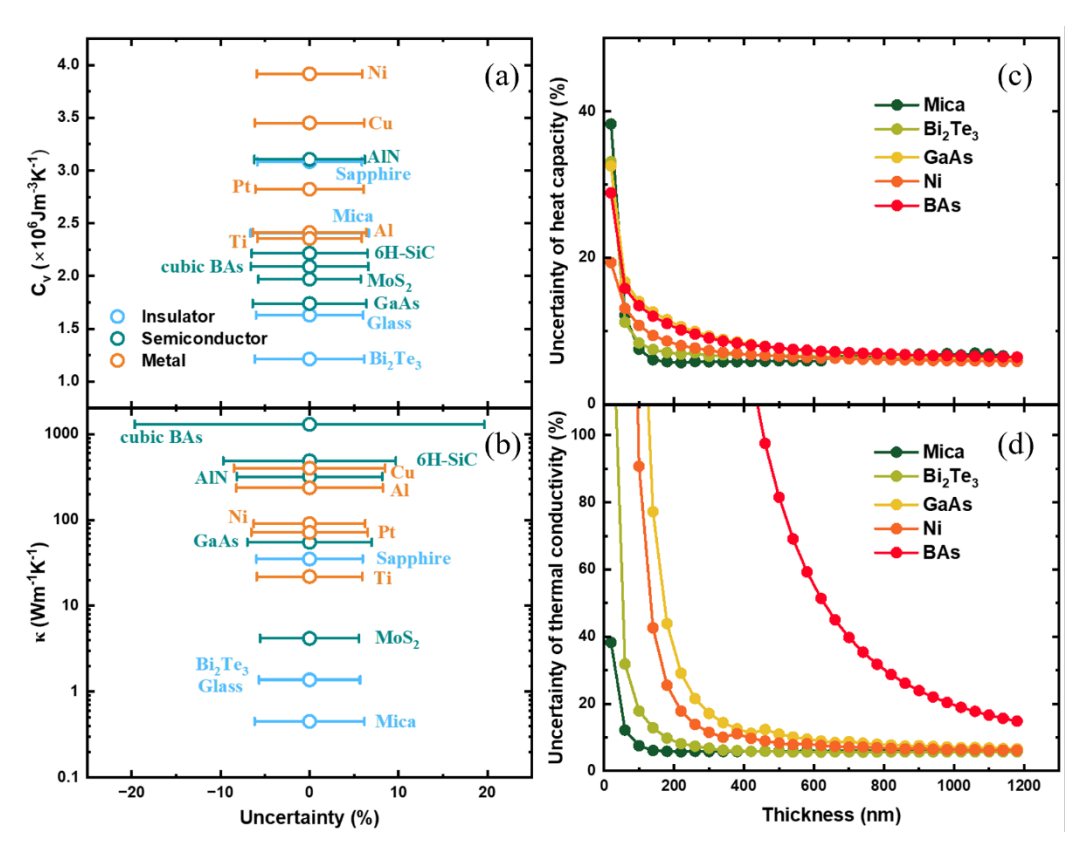


Figure 5. Uncertainty analysis on several representative materials [41], [43], [45]–[59]. (a) Materials with different c_v and their uncertainties. (b) Materials with different κ and their uncertainties. (c) Thicknesses dependent uncertainties of c_v for selected materials. (d) Thicknesses dependent uncertainties of κ .

We further calculate the uncertainties of different materials if measured with this combined approach. Since not all the materials are opaque and have short absorption depth, another gold layer is inserted between the material and the glass substrate as the absorption layer in ps-LF configurations. We use the 50nm-Au/Material/50nm-Au/Glass structure in all the simulations and calculate the uncertainties. Fig. 5a&b shows the uncertainties of 1 μ m-thick materials with different heat capacities and thermal conductivities. The uncertainties of the heat capacity are all below 20% and varies within a small range for most materials. There is no obvious relationship between uncertainties and the actual c_v values. The uncertainty of κ , on the other hand, is higher for larger κ , due to the faster heat penetration through the thin film and less effective time range. To determine the minimum thickness that can be possibly measured, we also calculate the uncertainties at different thicknesses (Fig. 5c&d). We define the minimum

thickness that our combined setup can measure are those at which both uncertainties of c_v and κ are below 20%. Overall, the uncertainties of the c_v drop below 20% at 50nm for all selected materials with wide c_v and κ range (Figure 5c). It is the uncertainty of κ that determines the minimum thickness. For materials with low thermal conductivity, such as Mica, the minimum thickness can be as small as 43nm. For ultrahigh thermal conductivity material, such as BAs, the minimum thickness is about 990nm. The minimum thickness could be further pushed to smaller values if the time resolution of data measurement can be improved. Currently, the resolution of our photodetector is 500ps. With a faster detector, more datapoints could be acquired that gives better performance during the fitting process, especially when the sample is thin. For very thick samples, high laser fluence is required, especially for the ps-LF measurement, so that the temperature rise on the probe side is high enough to give good signal-to-noise ratio. When laser fluence is too high, the Au transducer film could be damaged, which poses another restriction of this method, similar to traditional laser flash.

There are also other techniques to measure thermal conductivity of thin films such as the most common 3ω and TDTR (time domain thermoreflectance). The minimum thicknesses that 3ω can measure is limited by the thermal conductivity ratio between the film and the substrate and the width of the metal line, so it would be hard to measure the thermal conductivity of submicronthick thin film [44]. For TDTR, the minimum thickness that can be measured is governed by the smallest penetration depth. Accurate measurement of the thin film thermal conductivity requires the high sensitivity to the κ_{film} while low sensitivity to the substrate thermal conductivity, which means that the thermal penetration depth should be controlled as less than half of the thin film thickness. The thermal penetration depth d_{th} is reversely correlated to the modulation frequency fas $d_{th} = \sqrt{\frac{\alpha}{\pi f}}$, where α is the diffusivity of the film [60]. With the conventional TDTR, the maximum modulation frequency is usually 20MHz, beyond which the low output signal leads to large noise. Thus, the minimum thermal penetration depth is limited. Taking the Nickel case for comparison, the penetration depth of Ni at 20MHz is 668nm using the measured thermal conductivity and heat capacity. Jiang et al. extended the limitation of thin film measurement with TDTR through measuring two sets of data at different modulation frequencies and taking the signal ratio of these two measurements as the final signal for fitting [37]. This approach can improve the sensitivity of κ_{film} by suppressing the sensitivities of other parameters that are

always large in the high frequency range, such as the thickness of the transducer layer. The minimum thickness that this method can measure is $0.85d_{th}$, but the sensitivity of the thin film heat capacity is sacrificed. For Ni, this dual-frequency method can extend the minimum thickness to 567nm. With our combined approach, the Ni film measured has a thickness of 297nm Ni and both the thermal conductivity and heat capacity values are consistent to the previous work. Our combined technique offers unique advantages on measuring thermal properties with high accuracy. Another way is to treat the thin layer as the interface, but it requires the knowledge of the interfacial resistances between the thin film and adjacent layers (metal transducer and substrate) to extract the thermal conductivity, making the process even more complicated.

The combined approach described in this report offers unique advantages in characterizing thermal conductivity and heat capacity with low uncertainties, which have many potential applications in different research fields. Our experimental setup is compatible with most optically transparent chambers, including cryostat and diamond anvil cell (DAC), to enable in-situ thermal characterization at extreme conditions, where phase transition happens. Previous research has shown that the heat capacity measured by DSC and the thermal diffusivity by laser flash method near phase transition contain the contributions from both the lattice evolution and the phase transition [61], [62]. To extract the real thermal conductivity in this region, additional heat absorption term from the phase transition has to be added to the model to correct the heat transport equations [61]. Our combined setup can extract the total c_{ν} and k altogether, providing the true thermal conductivity value, and also separating the contributions from lattice evolution and phase transition, although further careful examination is still required.

Recently, phase change materials (PCMs) have been utilized in the chip thermal management due to the high latent heat that absorbs the heat and reduce the chip peak temperature. Among various PCM options, the solid-solid phase transition materials offer lower volume change and are container-free, leading to a more compact circuit design [63]. The thermal conductivities of PCMs range from 0.2 W/mK to 70 W/mK, while the heat capacities are between 0.7×10^6 J/m³K and 2.4×10^6 J/m³K, both are within the measurable range of our combined technique [64].

In Earth and planetary sciences, c_v and κ are crucial parameters to constrain heat flux efficiency of Earth' materials, and thus, help to understand the temperature and heat flux distribution in the interior of the Earth and other planets. While the combination between the DAC and TDTR or TTR are widely used in thermal conductivity measurements [65]–[69], previous measurements on heat capacity at high pressure usually used multi-anvil apparatus with millimeter-scale samples [70], [71]. By implementing a diamond anvil cell into our setup, it is now possible to measure c_v and κ on micron-sized materials under high pressure. This type of study would allow evaluation of thermal transport properties and heat capacity of candidate constituent minerals under high pressure and high temperature, thus enable understanding the heat transport, temperature distribution, and dynamic processes inside the planet.

In summary, we developed a combined approach with the ps-TTR and ps-LF methods for simultaneous determination of the heat capacity and thermal conductivity. Five metal films with thickness ranging from 297nm to $1.2\mu m$ are tested, with values consistent with literature data and uncertainties below $\pm 16\%$ and $\pm 8\%$ for thermal conductivity and heat capacity, separately. The low uncertainty mainly comes from the fact that the sensitivities of the heat capacity have different signs for ps-TTR and ps-LF, which cancel with each other in the matrix calculations. Considering the short optical absorption depth and zero band gap of the metal, no extra layer of gold between metal layer and glass layer is required for heat generation. While for other materials with either long optical absorption depth or band gap larger than pump laser wavelength, an extra layer of gold is needed to absorb the pump laser. Potential applications of the new methodology in thermal management, phase transitions in solid-state physics, and planetary sciences in extreme pressures and temperatures are discussed to highlight the potential impacts of the study.

- [1] F. Guillou *et al.*, "Non-hysteretic first-order phase transition with large latent heat and giant low-field magnetocaloric effect," *Nat. Commun.*, vol. 9, no. 1, 2018, doi: 10.1038/s41467-018-05268-4.
- [2] R. H. Busey, "Liquid and Gas. Heat of Fusion and Vaporization", vol. 75, no. 1952, pp.

- [3] V. K. Pecharsky, K. A. Gschneidner, and D. Fort, "Superheating and other unusual observations regarding the first order phase transition in Dy," *Scr. Mater.*, vol. 35, no. 7, pp. 843–848, 1996, doi: 10.1016/1359-6462(96)00225-4.
- [4] M. M. H. Polash, M. Rasoulianboroujeni, and D. Vashaee, "Magnon and spin transition contribution in heat capacity of ferromagnetic Cr-doped MnTe: Experimental evidence for a paramagnetic spin-caloritronic effect," *Appl. Phys. Lett.*, vol. 117, no. 4, 2020, doi: 10.1063/5.0011887.
- [5] A. Szewczyk, M. Gutowska, and B. Dabrowski, "Specific heat and phase diagram of heavily doped La1-xSrxMnO3 (0.45≤x≤1.0)," *Phys. Rev. B Condens. Matter Mater. Phys.*, vol. 72, no. 22, pp. 1–8, 2005, doi: 10.1103/PhysRevB.72.224429.
- [6] N. T. H. Kim-Ngan, S. Sowa, M. Krupska, M. Paukov, I. Tkach, and L. Havela, "Superconductivity in the splat-cooled UMo alloys," *Adv. Nat. Sci. Nanosci. Nanotechnol.*, vol. 6, no. 1, 2015, doi: 10.1088/2043-6262/6/1/015007.
- [7] J. Kačmarcík *et al.*, "Specific heat of superconducting MgCNi3 single crystals," *J. Phys. Conf. Ser.*, vol. 150, no. 5, pp. 3–7, 2009, doi: 10.1088/1742-6596/150/5/052087.
- [8] T. Katsura *et al.*, "Adiabatic temperature profile in the mantle," *Phys. Earth Planet. Inter.*, vol. 183, no. 1–2, pp. 212–218, 2010, doi: 10.1016/j.pepi.2010.07.001.
- [9] T. Katsura, "A Revised Adiabatic Temperature Profile for the Mantle," *J. Geophys. Res. Solid Earth*, vol. 127, no. 2, pp. 1–11, 2022, doi: 10.1029/2021JB023562.

- [10] W. P. Hsieh, E. Marzotto, Y. C. Tsao, T. Okuchi, and J. F. Lin, "High thermal conductivity of stishovite promotes rapid warming of a sinking slab in Earth's mantle," *Earth Planet. Sci. Lett.*, vol. 584, p. 117477, 2022, doi: 10.1016/j.epsl.2022.117477.
- [11] T. H. K. Barron, "Grüneisen parameters for the equation of state of solids," *Ann. Phys. (N. Y).*, vol. 1, no. 1, pp. 77–90, 1957, doi: https://doi.org/10.1016/0003-4916(57)90006-4.
- [12] E. Grüneisen, "Theorie des festen Zustandes einatomiger Elemente," *Ann. Phys.*, vol. 344, no. 12, pp. 257–306, 1912.
- [13] G. Mie, "Zur kinetischen Theorie der einatomigen Körper," *Ann. Phys.*, vol. 316, no. 8, pp. 657–697, 1903.
- [14] J. M. Walsh, M. H. Rice, R. G. McQueen, and F. L. Yarger, "Shock-wave compressions of twenty-seven metals. equations of state of metals," *Phys. Rev.*, vol. 108, no. 2, pp. 196–216, 1957, doi: 10.1103/PhysRev.108.196.
- [15] R. G. McQueen and S. P. Marsh, "Equation of state for nineteen metallic elements from shock-wave measurements to two megabars," *J. Appl. Phys.*, vol. 31, no. 7, pp. 1253–1269, 1960, doi: 10.1063/1.1735815.
- [16] F. A. Lindemann, "The calculation of molecular vibration frequencies," *Phys. Zeitschrift*, vol. 11, no. 0369-982X, pp. 609–612, 1910, [Online]. Available: https://ntrs.nasa.gov/api/citations/19840027015/downloads/19840027015.pdf
- [17] T. H. and F. R.A., Eds., *Deep Earth: Physics and Chemistry of the Lower Mantle and Core*. American Geophysical Union / John Wiley and Sons, 2016. [Online]. Available: http://onlinelibrary.wiley.com/book/10.1002/9781118992487

- [18] D. G. Cahill, "Analysis of heat flow in layered structures for time-domain thermoreflectance," *Rev. Sci. Instrum.*, vol. 75, no. 12, pp. 5119–5122, Dec. 2004, doi: 10.1063/1.1819431.
- [19] W. J. Parker, R. J. Jenkins, C. P. Butler, and G. L. Abbott, "Flash method of determining thermal diffusivity, heat capacity, and thermal conductivity," *J. Appl. Phys.*, vol. 32, no. 9, pp. 1679–1684, 1961, doi: 10.1063/1.1728417.
- [20] T. B. and A. Ono, "Improvement of the laser flash method to reduce uncertainty in thermal diffusivity measurements," 2001. [Online]. Available: www.iop.org
- [21] N. Taketoshi, T. Baba, and A. Ono, "Observation of Heat Diffusion across Submicrometer Metal Thin Films Using a Picosecond Thermoreflectance Technique," Publication Board, 1999.
- [22] N. Taketoshi, T. Baba, and A. Ono, "Development of a thermal diffusivity measurement system for metal thin films using a picosecond thermoreflectance technique," 2001.[Online]. Available: www.iop.org
- [23] N. Taketoshi, T. Baba, and A. Ono, "Electrical delay technique in the picosecond thermoreflectance method for thermophysical property measurements of thin films," *Rev. Sci. Instrum.*, vol. 76, no. 9, Sep. 2005, doi: 10.1063/1.2038628.
- [24] T. Baba, N. Taketoshi, and T. Yagi, "Development of ultrafast laser flash methods for measuring thermophysical properties of thin films and boundary thermal resistances," in *Japanese Journal of Applied Physics*, Nov. 2011, vol. 50, no. 11 PART 2. doi: 10.1143/JJAP.50.11RA01.

- [25] T. Yagi, K. Tamano, Y. Sato, N. Taketoshi, T. Baba, and Y. Shigesato, "Analysis on thermal properties of tin doped indium oxide films by picosecond thermoreflectance measurement," *J. Vac. Sci. Technol. A Vacuum, Surfaces, Film.*, vol. 23, no. 4, pp. 1180– 1186, 2005, doi: 10.1116/1.1872014.
- [26] T. Baba, "Analysis of one-dimensional heat diffusion after light pulse heating by the response function method," *Jpn. J. Appl. Phys.*, vol. 48, no. 5 PART 3, May 2009, doi: 10.1143/JJAP.48.05EB04.
- [27] L. Chen, A. M. Limarga, and D. R. Clarke, "A new data reduction method for pulse diffusivity measurements on coated samples," *Comput. Mater. Sci.*, vol. 50, no. 1, pp. 77–82, Nov. 2010, doi: 10.1016/j.commatsci.2010.07.009.
- [28] K. Hatori, N. Taketoshi, T. Baba, and H. Ohta, "Thermoreflectance technique to measure thermal effusivity distribution with high spatial resolution," *Rev. Sci. Instrum.*, vol. 76, no. 11, pp. 1–7, 2005, doi: 10.1063/1.2130333.
- [29] R. Garrelts, A. Marconnet, and X. Xu, "Assessment of Thermal Properties via Nanosecond Thermoreflectance Method," *Nanoscale Microscale Thermophys. Eng.*, vol. 19, no. 4, pp. 245–257, 2015, doi: 10.1080/15567265.2015.1078425.
- [30] J. Jeong *et al.*, "Picosecond transient thermoreflectance for thermal conductivity characterization," *Nanoscale Microscale Thermophys. Eng.*, vol. 23, no. 3, pp. 211–221, Jul. 2019, doi: 10.1080/15567265.2019.1580807.
- [31] A. J. Schmidt, X. Chen, and G. Chen, "Pulse accumulation, radial heat conduction, and anisotropic thermal conductivity in pump-probe transient thermoreflectance," *Rev. Sci. Instrum.*, vol. 79, no. 11, 2008, doi: 10.1063/1.3006335.

- [32] A. J. Schmidt, R. Cheaito, and M. Chiesa, "A frequency-domain thermoreflectance method for the characterization of thermal properties," *Rev. Sci. Instrum.*, vol. 80, no. 9, 2009, doi: 10.1063/1.3212673.
- [33] J. Yang, C. Maragliano, and A. J. Schmidt, "Thermal property microscopy with frequency domain thermoreflectance," *Rev. Sci. Instrum.*, vol. 84, no. 10, 2013, doi: 10.1063/1.4824143.
- [34] J. B. Henderson, J. A. Wiebelt, and M. R. Tant, "A method for the determination of the specific heat and heat of decomposition of composite materials," *Thermochim. Acta*, vol. 57, pp. 161–171, 1982.
- [35] M. J. O'Neill, "Measurement of Specific Heat Functions by Differential Scanning Calorimetry," *Anal. Chem.*, vol. 38, no. 10, pp. 1331–1336, 1966, doi: 10.1021/ac60242a011.
- [36] J. Liu, J. Zhu, M. Tian, X. Gu, A. Schmidt, and R. Yang, "Simultaneous measurement of thermal conductivity and heat capacity of bulk and thin film materials using frequencydependent transient thermoreflectance method," *Rev. Sci. Instrum.*, vol. 84, no. 3, Mar. 2013, doi: 10.1063/1.4797479.
- [37] P. Jiang, B. Huang, and Y. K. Koh, "Accurate measurements of cross-plane thermal conductivity of thin films by dual-frequency time-domain thermoreflectance (TDTR)," *Rev. Sci. Instrum.*, vol. 87, no. 7, 2016, doi: 10.1063/1.4954969.
- [38] R. B. Wilson, B. A. Apgar, L. W. Martin, and D. G. Cahill, "Thermoreflectance of metal transducers for optical pump-probe studies of thermal properties," *Opt. Express*, vol. 20, no. 27, p. 28829, 2012, doi: 10.1364/oe.20.028829.

- [39] I. H. Chowdhury and X. Xu, "Heat transfer in femtosecond laser processing of metal," *Numer. Heat Transf. Part A Appl.*, vol. 44, no. 3, pp. 219–232, 2003, doi: 10.1080/716100504.
- [40] L. Guo, S. L. Hodson, T. S. Fisher, and X. Xu, "Heat transfer across metal-dielectric interfaces during ultrafast-laser heating," *J. Heat Transfer*, vol. 134, no. 4, pp. 1–5, 2012, doi: 10.1115/1.4005255.
- [41] Y. S. Touloukian and E. H. Buyco, *Thermophysical Properties of Matter The TPRC Data Series. Volume 4. Specific Heat Metallic Elements and Alloys*, vol. 4, no. Specific Heat. 1971.
- [42] Y. S. Touloukian, R. K. Kirby, R. E. Taylor, and P. D. Desai, *Thermophysical Properties of Matter The TPRC Data Series. Volume 1. Thermal Conductivity Metallic Elements and Alloys.* 1970.
- [43] C. Y. Ho, R. W. Powell, and P. E. Liley, "Thermal Conductivity of the Elements: A Comprehensive Review," *J. Phys. Chem. Ref. Data*, vol. 3, 1974, doi: 10.1063/1.3253100.
- [44] Y. K. Koh *et al.*, "Comparison of the 3ω method and time-domain thermoreflectance for measurements of the cross-plane thermal conductivity of epitaxial semiconductors," *J. Appl. Phys.*, vol. 105, no. 5, 2009, doi: 10.1063/1.3078808.
- [45] J. Yang, E. Ziade, and A. J. Schmidt, "Uncertainty analysis of thermoreflectance measurements," *Rev. Sci. Instrum.*, vol. 87, no. 1, 2016, doi: 10.1063/1.4939671.
- [46] J. S. Kang, M. Li, H. Wu, H. Nguyen, and Y. Hu, "Experimental observation of high thermal conductivity in boron arsenide," *Science* (80-.)., vol. 361, no. 6402, pp. 575–578,

- 2018, doi: 10.1126/science.aat5522.
- [47] N. P. Gorbachuk and V. R. Sidorko, "Heat capacity and enthalpy of Bi2Si3 and Bi2Te3 in the temperature range 58-1012 K," *Poroshkovaya Metall.*, vol. 43, no. 5–6, pp. 79–86, 2004.
- [48] I. T. Witting *et al.*, "The Thermoelectric Properties of Bismuth Telluride," *Adv. Electron. Mater.*, vol. 5, no. 6, pp. 1–20, 2019, doi: 10.1002/aelm.201800904.
- [49] J. S. Blakemore, "Semiconducting and other major properties of gallium arsenide," *J. Appl. Phys.*, vol. 53, no. 10, 1982, doi: 10.1063/1.331665.
- [50] H. J. Goldsmid and A. E. Bowley, "Thermal conduction in mica along the planes of cleavage," *Nature*, vol. 187, no. 4740, pp. 864–865, 1960.
- [51] A. S. Gray and C. Uher, "Thermal conductivity of mica at low temperatures," *J. Mater. Sci.*, vol. 12, no. 5, pp. 959–965, 1977, doi: 10.1007/BF00540978.
- [52] A. Bano, P. Khare, and N. K. Gaur, "Thermal transport properties of bulk and monolayer MoS2: An ab-initio approach," *J. Phys. Conf. Ser.*, vol. 836, no. 1, 2017, doi: 10.1088/1742-6596/836/1/012052.
- [53] V. Varshney, S. S. Patnaik, C. Muratore, A. K. Roy, A. A. Voevodin, and B. L. Farmer, "MD simulations of molybdenum disulphide (MoS2): Force-field parameterization and thermal transport behavior," *Comput. Mater. Sci.*, vol. 48, no. 1, pp. 101–108, 2010, doi: 10.1016/j.commatsci.2009.12.009.
- [54] D. A. Ditmars, S. Ishihara, S. S. Chang, G. Bernstein, and E. D. West, "ENTHALPY

- AND HEAT-CAPACITY STANDARD REFERENCE MATERIAL: SYNTHETIC SAPPHIRE (alpha -Al2O3) FROM 10 TO 2250 K.," *J. Res. Natl. Bur. Stand. (United States)*, vol. 87, no. 2, pp. 159–163, 1982, doi: 10.6028/jres.087.012.
- [55] P. Jiang, X. Qian, X. Gu, and R. Yang, "Probing Anisotropic Thermal Conductivity of Transition Metal Dichalcogenides MX2 (M = Mo, W and X = S, Se) using Time-Domain Thermoreflectance," *Adv. Mater.*, vol. 29, no. 36, pp. 1–7, 2017, doi: 10.1002/adma.201701068.
- [56] F. Medjdoub and K. Iniewski, "Gallium Nitride (GaN)," *Gallium Nitride (GaN)*. 2017. doi: 10.4324/b19387.
- [57] B. Salce, L. Devoille, R. Calemczuk, A. I. Buzdin, G. Dhalenne, and A. Revcolevschi, "Thermal conductivity of pure and Si-doped CuGeO3," *Phys. Lett. Sect. A Gen. At. Solid State Phys.*, vol. 245, no. 1–2, pp. 127–132, 1998, doi: 10.1016/S0375-9601(98)00347-8.
- [58] L. Boteler, A. Lelis, M. Berman, and M. Fish, "Thermal conductivity of power semiconductors-when does it matter?," 2019 IEEE 7th Work. Wide Bandgap Power Devices Appl. WiPDA 2019, pp. 265–271, 2019, doi: 10.1109/WiPDA46397.2019.8998802.
- [59] F. James, E. J. F. Shackelford, and W. Alexander, *Materials Science Engineering Hand Book*, vol. 232. 2001. [Online]. Available: http://www.fulviofrisone.com/attachments/article/372/Materials Science and Engineering Handbook.pdf%0Ahttp://scholar.google.com/scholar?hl=en&btnG=Search&q=intitle:mat erials+science+and+engineering+handbook#0
- [60] P. Jiang, X. Qian, and R. Yang, "A new elliptical-beam method based on time-domain thermoreflectance (TDTR) to measure the in-plane anisotropic thermal conductivity and

- its comparison with the beam-offset method," *Rev. Sci. Instrum.*, vol. 89, no. 9, 2018, doi: 10.1063/1.5029971.
- [61] H. Chen *et al.*, "Thermal Conductivity during Phase Transitions," *Adv. Mater.*, vol. 31, no. 6, pp. 1–7, 2019, doi: 10.1002/adma.201806518.
- [62] M. T. Agne, P. W. Voorhees, and G. J. Snyder, "Phase Transformation Contributions to Heat Capacity and Impact on Thermal Diffusivity, Thermal Conductivity, and Thermoelectric Performance," *Adv. Mater.*, vol. 31, no. 35, pp. 1–7, 2019, doi: 10.1002/adma.201902980.
- [63] C. R. Raj, S. Suresh, R. R. Bhavsar, and V. K. Singh, "Recent developments in thermophysical property enhancement and applications of solid solid phase change materials: A review," *J. Therm. Anal. Calorim.*, vol. 139, no. 5, pp. 3023–3049, 2020, doi: 10.1007/s10973-019-08703-w.
- [64] W. Hua, L. Zhang, and X. Zhang, "Research on passive cooling of electronic chips based on PCM: A review," *J. Mol. Liq.*, vol. 340, p. 117183, 2021, doi: 10.1016/j.molliq.2021.117183.
- [65] W. P. Hsieh and D. G. Cahill, "Ta and Au(Pd) alloy metal film transducers for time-domain thermoreflectance at high pressures," *J. Appl. Phys.*, vol. 109, no. 11, 2011, doi: 10.1063/1.3592882.
- [66] W. P. Hsieh, "Thermal conductivity of methanol-ethanol mixture and silicone oil at high pressures," *J. Appl. Phys.*, vol. 117, no. 23, 2015, doi: 10.1063/1.4922632.
- [67] W. P. Hsieh, B. Chen, J. Li, P. Keblinski, and D. G. Cahill, "Pressure tuning of the

- thermal conductivity of the layered muscovite crystal," *Phys. Rev. B Condens. Matter Mater. Phys.*, vol. 80, no. 18, pp. 1–4, 2009, doi: 10.1103/PhysRevB.80.180302.
- [68] X. Meng *et al.*, "Thermal Conductivity Enhancement in MoS2 under Extreme Strain," *Phys. Rev. Lett.*, vol. 122, no. 15, p. 155901, 2019, doi: 10.1103/PhysRevLett.122.155901.
- [69] Y. Zhou *et al.*, "Defect-modulated thermal transport behavior of BAs under high pressure," *Appl. Phys. Lett.*, vol. 121, no. 12, 2022, doi: 10.1063/5.0113007.
- [70] M. Osako *et al.*, "Thermal diffusivity, thermal conductivity and heat capacity of serpentine (antigorite) under high pressure," *Phys. Earth Planet. Inter.*, vol. 183, no. 1–2, pp. 229–233, 2010, doi: 10.1016/j.pepi.2010.07.005.
- [71] Y. Xu, T. J. Shankland, S. Linhardt, D. C. Rubie, F. Langenhorst, and K. Klasinski, "Thermal diffusivity and conductivity of olivine, wadsleyite and ringwoodite to 20 GPa and 1373 K," *Phys. Earth Planet. Inter.*, vol. 143, no. 1–2, pp. 321–336, 2004, doi: 10.1016/j.pepi.2004.03.005.